Crystallographic tilting during heteroepitaxial growth of rubidium iodide on mica

F. J. Lamelas,* May Xiong, and C. V. Sloane
Department of Physics, Marquette University, Milwaukee, Wisconsin 53233
(Received 17 February 2000)

Heteroepitaxial deposits of RbI on mica were prepared by the evaporation of aqueous solutions under controlled conditions. Using four-circle x-ray diffractometer measurements to determine the orientation of the alkali halide lattice relative to the mica substrate, we find that the RbI [111] axis is often tilted relative to the substrate normal, along specific in-plane azimuths. Crystallographic tilting is a well-known phenomenon during heteroepitaxial growth of semiconductors and metals, but our results are somewhat unusual, since they involve the growth of an ionic crystal on mica. It is generally acknowledged that tilting is driven by epitaxial misfit accommodation, and for a net tilt to occur the interfacial system requires a symmetry-breaking component. In the vast majority of previous studies the broken symmetry is due to substrate miscut, but miscut is entirely absent in the case of cleaved mica substrates. In order to explain our results, we show that the tilting of RbI on mica is made possible by the inherent threefold symmetry of the [111] axis in fcc crystals, and we also show that the observed tilt angles are consistent with the lattice parameters of RbI and mica.

I. INTRODUCTION

Most surface science and epitaxial growth experiments are carried out in vacuum or partial-vacuum environments, as are many processes used in the production of electronic and optoelectronic materials. On the other hand, crystal growth from solution occurs in many natural systems and in a variety of commercial processes. Detailed experimental studies of growth from solution are relatively uncommon, but in recent years a variety of new approaches have revealed an increasing number of interesting phenomena. Notable examples include an x-ray scattering study of the structure of a potassium dihydrogen phosphate crystal surface in contact with its growth solution,[1] and atomic-force-microscope studies of the growth dynamics of calcite crystals.[2] In another study of calcite growth, patterned self-assembled organic monolayers have been used in the production of ordered arrays of crystals with a variety of controlled orientations relevant to the substrate normal.[3] In experiments that could lead to electronic applications, heteroepitaxially oriented bismuth oxide has been grown on gold,[4] and zinc oxide has been grown on gallium nitride.[5]

In a recent study, motivated by an interest in unusual epitaxial growth environments, we have examined the deposition of alkali halides on mica during the evaporation of aqueous solutions.[6] As a model system that can be used to study growth morphologies, rubidium iodide on mica is attractive, given the small epitaxial mismatch and the relative simplicity of the growth process. In our earlier experiments, the evaporation was carried out with the substrates exposed to ambient air, with control over the substrate temperature but no independent control of the evaporation rate. Reference 6 included data on the morphology of epitaxial RbI islands, as revealed by optical and force microscopy, and also x-ray scattering measurements of the degree of the azimuthal orientation with respect to the mica substrate. The collective results of those measurements made it clear that this growth system is quite robust, in that oriented growth occurs over a wide range of conditions, including fast evaporation at temperatures approaching 100 °C.

Our present study is an extension of the initial experiments with better control of the growth conditions. To this end we have constructed a cell that allows independent control of the substrate temperature and the evaporation rate. We have repeated many of the measurements of the previous study and have obtained interesting results of two types. The first result involves the macroscopic morphology of epitaxial islands and will be reported elsewhere. The second result, which is the subject of this paper, concerns the microscopic structure of the substrate-overlayer interface and the tilting of the overlayer [111] axis relative to the substrate normal.

Crystal tilting at heteroepitaxial interfaces has been studied for at least a quarter of a century.[7] Specific tilt systems have included compound semiconductor overlayers,[7–9] Si-Ge alloys,[10] and semiconductors in general.[11] The phenomenon has also been observed in heteroepitaxy of metals.[12] Although details vary from model to model, the general consensus is that tilting occurs during the accommodation of misfit at heterointerfaces. In systems where misfit stresses are relieved via dislocation motion, a symmetric set of easy slip planes will produce dislocations but no net tilt, since there is no favored tilt direction. Therefore, the preferential glide model of Ayers *et al.*[11] includes a symmetry-breaking component, consisting of the miscut of the substrate crystal along a low-index in-plane azimuth. Other proposed tilt models, such as those reviewed by Riesz *et al.*,[9] also require a vicinal substrate surface. The RbI-on-mica system is somewhat unusual, given the material system (an ionic crystal on mica) and the growth environment (precipitation from a supersaturated solution). In addition, the cleaved mica surface corresponds to a substrate with *zero miscut*; therefore the required symmetry-breaking must be found elsewhere. As we will show below, the asymmetry that leads to a tilt of the RbI islands is an intrinsic property of an untwinned rocksalt structure. We will also show that the observed tilt angles are consistent with previously published lattice parameters of RbI and mica.

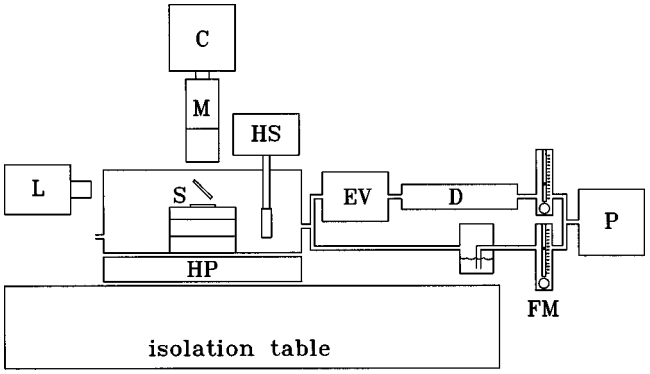

FIG. 1. Diagram of the sample growth system. Starting from the right, compressed air is provided by an oil-free pump (P) and is split into two lines monitored by flow meters. In the wet line (below), the air passes through a water bath, and in the dry line the air passes through a desiccant (D) and a computer-controlled electric valve (EV). The sample (S) is mounted in the growth cell, which contains a humidity sensor (HS). Using a beam splitter, the sample is illuminated by a lamp (L) and growth-run images are recorded using a microscope (M) and a video camera. The system is vibration isolated, and for high-dew-point runs the entire cell is heated by a hot plate.

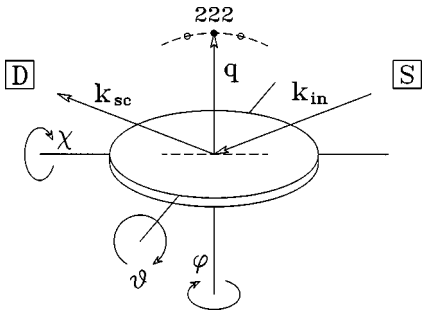

FIG. 2. X-ray scattering geometry. A source (S) produces a monochromatic incident beam with wave vector $\vec{k}_{in}$, and the scattered beam ($\vec{k}_{sc}$) is measured by a detector (D). In a θ rocking scan the tip of the scattering vector $\vec{q}$ sweeps across the dashed arc. Epitaxial RbI deposits with the [111] axis normal to the substrate would produce a 222 reflection at the position of the filled circle, but tilted deposits produce 222 reflections at off-specular positions, as indicated schematically by the open circles. The azimuthal direction of the tilt is determined by performing a series of θ scans at different fixed values of ϕ. The dashed line at the center of the disk corresponds to the projection of the θ-scan trajectory onto the substrate surface.

II. EXPERIMENTAL METHODS

When an aqueous solution of RbI is evaporated on mica, the solution becomes supersaturated and epitaxial islands form, as a consequence of the close match between RbI (111) planes and the mica cleavage surface. The interfacial misfit that is predicted by the published lattice parameters of muscovite mica[13] and RbI (Ref. 14) is $\sim 0.2\%$. Our samples were prepared by the evaporation of single drops of a 2% RbI solution on cleaved mica substrates placed in the growth cell of Fig. 1. The important features of this cell include temperature control, using a Peltier stage operated in either heating or cooling mode, and control of the dew point, using a humidity sensor and computer-controlled air flows. Control of the temperature affects transport kinetics during growth, and control of the dew point affects the evaporation rate and therefore the deposition rate.

At a given temperature, the physical rate-limiting parameter is the supersaturation of the RbI solution, but we have no direct measurement of the supersaturation in these experiments. For convenience, we employ a qualitative measure of the growth rate which is defined as $\Delta = T_{ss} - T_d$, where T_{ss} is the substrate temperature and T_d is the dew point. Small and large values of Δ correspond to slow and fast evaporation of the salt solution, and therefore slow and fast growth rates. In practice, we find that the evaporation rate drops to zero at values of Δ in the neighborhood of 5 °C. (The evaporation rate of a drop of pure water would drop to zero at $\Delta = 0$, but the vapor pressure of water is lowered in equilibrium with a saturated salt solution.) The minimum dew point that can be attained is that of the dry-air line; in our setup a value of approximately -20 °C was obtained using standard desiccants. For those runs in which the dew point in the cell is higher than room temperature, it is necessary to heat the entire cell in order to avoid condensation on its walls; the maximum dew point that can be reached comfortably with our setup is approximately 70 °C. The substrate temperatures that we used varied between 0 and 90 °C.

The external morphology of the RbI islands was monitored during growth using optical microscopy. In most cases the RbI formed triangular islands similar to those shown in Ref. 6. The triangular shape corresponds to a (111) basal plane; the upper surfaces of the islands tend to form a pyramid with low-energy {100} faces. (The orientation of the RbI islands relative to the mica substrate is shown in Fig. 11 below.) Following growth, the samples were stored in desiccators and subsequently exposed to ambient humidity during x-ray measurements. Scans performed months after the initial measurements indicated that the structures discussed in this paper are stable.

The x-ray measurements were performed using a Cu $K\alpha$ tube source operated at 1 kW ($\lambda \sim 1.54$ Å). The beam was reflected from a flat pyrolytic graphite monochromator, with slits used to narrow the horizontal divergence to 0.08°, a value significantly smaller than the mosaic spread of the monochromator. The vertical beam divergence was much broader; a χ scan through Si 004 had a width of 1.62°. These settings produced the elongated instrumental resolution function discussed in the following section. X rays were counted with a scintillation detector, using counting times of 5 s per point. The full set of scans performed for each sample was usually carried out over 6.5 h.

Disk-shaped samples with a typical diameter of 10 mm were mounted with the plane of the sample normal to the ϕ axis of a four-circle diffractometer, aligned, using laser reflection from the mica substrate, to an accuracy of $\sim 0.1°$. The scattering plane, shown in Fig. 2, was horizontal. The x-ray data discussed in this paper are confined to θ rocking scans, where the incident and scattered beam directions are fixed and the sample is rotated about the θ axis. In these scans the trajectory of the scattering vector is along the dashed arc shown in Fig. 2. By adjusting the ϕ setting, it is possible to place the θ-scan trajectory along specific in-plane azimuths, as discussed in the following section.

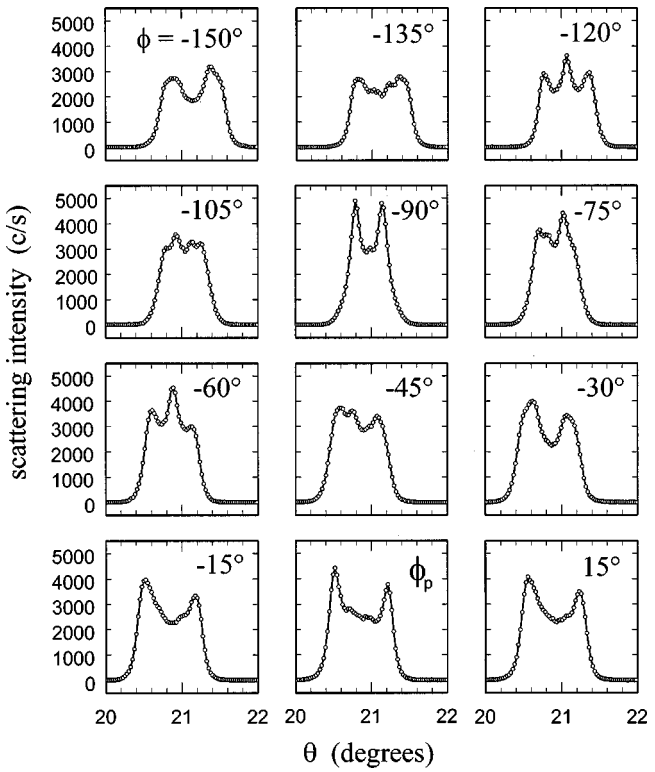

FIG. 3. A series of θ rocking scans performed with a sample grown at $T_{ss}=20\,^{\circ}\mathrm{C}$, $T_d=-18.5\,^{\circ}\mathrm{C}$, and $\Delta=38.5\,^{\circ}\mathrm{C}$. The scan with the widest peak splitting (bottom row, center) is labeled ϕ_p and the azimuths of all other scans are labeled relative to ϕ_p.

III. MEASUREMENTS OF TILT DISTRIBUTIONS

A RbI deposit with zero tilt relative to the substrate plane would result in a single peak in a θ scan, as shown in Fig. 2. If all RbI islands were tilted with an identical orientation one would also measure a single peak, with $\vec{q}$ rotated away from the substrate normal. If multiple tilt orientations occur, one expects a corresponding number of peaks in the θ scan, as indicated by the open circles of Fig. 2. Suppose that several epitaxial tilts occur along a single azimuthal orientation. In the case of perfect instrumental resolution, one would obtain multiple peaks in a θ scan only with a ϕ setting that places the scan trajectory exactly along the tilt direction. Two complications occur in our measurements of RbI on mica. First of all, the resolution function is elongated in a direction normal to the scan trajectory, and secondly, the actual distribution of tilt orientations occurs along multiple ϕ azimuths.

In order to explain our interpretation of the θ-scan measurements, we turn to the specific data set shown in Fig. 3 for a sample grown with $T_{ss}=20\,^{\circ}\mathrm{C}$, $T_d=-18.5\,^{\circ}\mathrm{C}$, and $\Delta=38.5\,^{\circ}\mathrm{C}$. All of the intensities correspond to the RbI 222 peak, with the observed scan profiles arising from islands with varying orientations relative to the substrate normal. The individual plots in Fig. 3 correspond to θ scans performed at 15° increments in ϕ settings. Qualitatively, it is clear that pronounced peak splittings occur at many azimuths, with splittings and widths that vary from scan to scan. The scan with the largest splitting (bottom row, center) is labeled ϕ_p and all other ϕ azimuths are referenced to that position.

The first ϕ setting of Fig. 3 (top row, left) was chosen so as to place the scan trajectory along a RbI $\langle 1\bar{1}0\rangle$ axis, and subsequent scans were performed after successive 15° ϕ rotations. An untwinned fcc crystal has three-fold symmetry about its [111] axis, and therefore one might expect that the θ scans would traverse an equivalent RbI axis after 120° ϕ rotations. On the other hand, θ scans performed after 180° ϕ rotations are equivalent, but reversed in direction. In addition, as shown in Ref. 6, the RbI islands occur in two azimuthal orientations corresponding to the two possible (111) stacking twins.[15] The result is that θ-scan trajectories along RbI $\langle 1\bar{1}0\rangle$ occur every 60° in ϕ. The other low-index directions in the (111) plane are $\langle 11\bar{2}\rangle$; these occur 30° from the $\langle 1\bar{1}0\rangle$ scans. In Fig. 3, the scans with trajectories along $\langle 1\bar{1}0\rangle$ are labeled $\phi=-150°$, $-90°$, and $-30°$, and the scans along $\langle 11\bar{2}\rangle$ are labeled $\phi=-120°$, $-60°$, and ϕ_p.

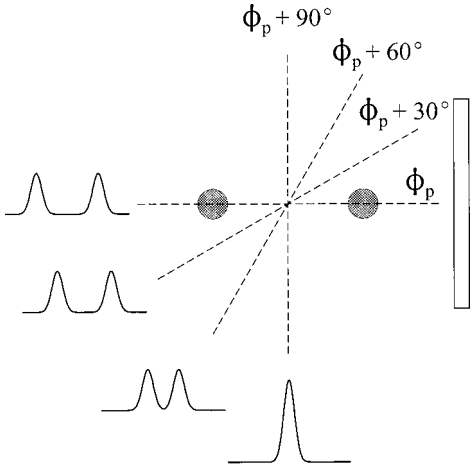

FIG. 4. Diagram of the expected intensity profiles in the case of tilting along a single azimuth. It is assumed that the resolution function (indicated by the narrow rectangle) is elongated in the direction normal to the scan trajectory. In this case, the largest peak splitting will be observed when the scan trajectory is along ϕ_p, with progressively smaller splittings as the scan trajectory approaches $\phi_p+90°$.

One might think, given the sixfold ϕ symmetry implied by the previous arguments, that a corresponding symmetry should occur in the θ-scan data, but the data of Fig. 3 do not have this symmetry. This is due to the influence of the mica substrate, which has only twofold symmetry. Since the tilting is caused by interfacial misfit, the θ-scan peak splittings are different along mica [100] and mica [010]. The scan with the broadest peak splitting in Fig. 3, labeled ϕ_p, has a trajectory along mica [010] and RbI $\langle 11\bar{2}\rangle$.

In order to interpret the intensity profiles of Fig. 3, we turn to specific models of tilt distributions. Figure 4 shows an idealized case where two tilt orientations occur along a single azimuth, as indicated by the filled circles. The resolution function, which is determined by the horizontal and vertical incident-beam divergences, is narrow in the direction of the scan trajectory and broad in the direction normal to the scan trajectory. During a θ scan, the resolution function (shown as an elongated rectangle to the right) sweeps across the dashed line corresponding to the scan trajectory, with the long axis of the resolution function normal to the scan trajectory. If the resolution function is long enough, both peaks

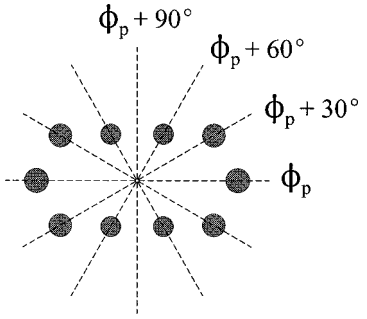

FIG. 5. Model of intrinsic peak splittings used in fitting the data of Fig. 3. Splittings occur along three separate azimuths, with weightings proportional to the areas of the shaded circles. The radial position of a given circle corresponds to the tilt angle along the corresponding azimuth.

will be detected, regardless of the azimuthal orientation of the scan, but the measured peak splittings will vary until, in a scan along the vertical ($\phi_p + 90°$) trajectory, both peaks coincide. It is clear that the intensities of Fig. 3 are too complex to be explained by the model of Fig. 4. In particular, since the peak splitting persists even at $\phi = \phi_p - 90°$ (Fig. 3, second row, center), the observed epitaxial tilts occur along *several* azimuths.

A more complex model, developed through trial and error, is shown in Fig. 5. This tilt distribution includes different weightings and tilt angles along three separate azimuths. Specifically, the tilt angles along the three azimuths are 0.42°, 0.37°, and 0.22°, and the corresponding weightings are 1.0, 0.9, and 0.7. To model the scattering intensities, we calculate the convolution of the Fig. 5 distribution with a resolution function qualitatively similar to that of Fig. 4. To minimize the number of free parameters and simplify the calculation, we assume that the resolution function is constant along the long axis and has a Gaussian shape in the narrow direction, with the width of the Gaussian fixed at 0.15° in order to match the experimental data. In Fig. 6 we plot the intensities derived from the model along with the data from four high-symmetry scans of Fig. 3. (All calculations in Fig. 6 are performed with the same set of model parameters.)

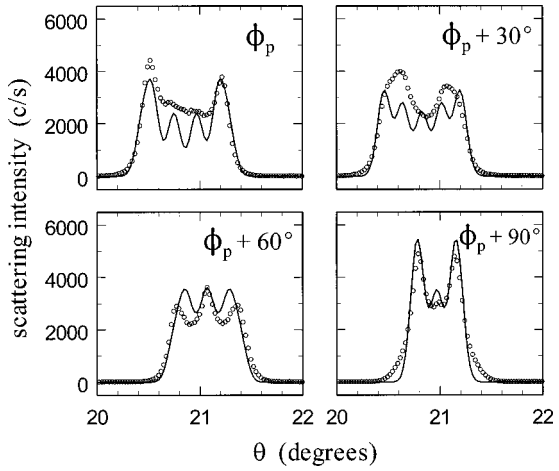

FIG. 6. Selected data from Fig. 3 (points), and calculated intensities (curves). The calculations employed the tilt distribution of Fig. 5, following the procedure described in the text.

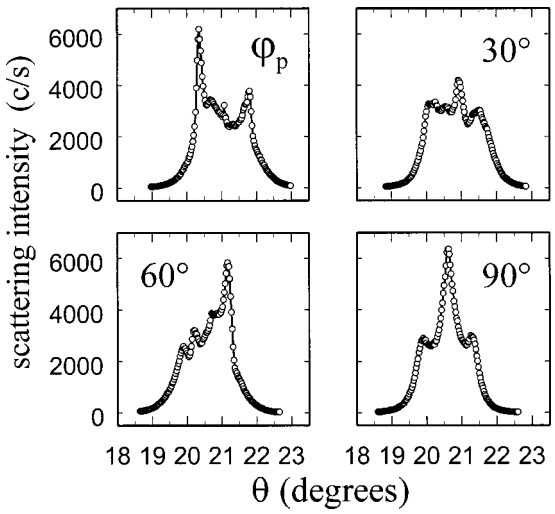

FIG. 7. Disordered peak-splitting structure for a sample grown at a relatively low growth rate, with $T_{ss} = 30\,°\mathrm{C}$, $T_d = 25\,°\mathrm{C}$, and $\Delta = 5\,°\mathrm{C}$.

The fit to the θ-scan data is not exact but it reproduces the character of the measurements. Our model of the tilt distributions is not necessarily unique, in that other distributions may fit the data as well as that in Fig. 6; however two basic conclusions may be derived from our analysis. First, it is clear that tilting occurs, given data such as those of Fig. 3. Secondly, the distribution of tilt orientations is qualitatively similar to the model of Fig. 5, in that there is tilting along a preferred azimuth (along ϕ_p) and also along other azimuths, with the preferred tilt azimuth coinciding with the largest peak splitting.

Sets of 12 θ scans at azimuthal increments of 15° were collected for samples grown over the full range of accessible growth conditions. In Fig. 7 we show θ scans for a sample grown at a low growth rate, with $T_{ss} = 30\,°\mathrm{C}$, $T_d = 25\,°\mathrm{C}$, and $\Delta = 5\,°\mathrm{C}$. The tilting behavior persists under these conditions, and in fact the tilt angle along the preferential tilt direction is relatively large (0.7°), but the distributions of tilt orientations are disordered, relative to those of Fig. 6. In other cases, the tilting behavior is partially suppressed, as shown in Fig. 8 for a sample grown with $T_{ss} = 40.1\,°\mathrm{C}$, $T_d = 30\,°\mathrm{C}$, and $\Delta = 10.1\,°\mathrm{C}$. In this case the peaks at the centers of the θ scans correspond to an untilted component of the island distribution. At high temperatures and growth rates, the tilting tends to vanish completely, as in the case of Fig. 9, which contains data for a sample with $T_{ss} = 59.4\,°\mathrm{C}$, $T_d = -8\,°\mathrm{C}$, and $\Delta = 67.4\,°\mathrm{C}$.

The collective tilt behavior is summarized in Fig. 10, which is based on the data taken with all of our samples. We have characterized each sample using its scan at $\phi = \phi_p$, and, in those cases where a peak splitting was observed, an open circle is plotted with a diameter proportional to the tilt angle. For samples where the θ scan seems to contain a single component, a filled circle is shown with a diameter proportional to the peak width. The general trend in Fig. 10 is that the peak splitting is suppressed as the growth rate and substrate temperature are increased. In particular, the splitting vanished in samples grown at 0, 10, and 60 °C at high rates, and there is almost no splitting in samples grown at 90 °C.

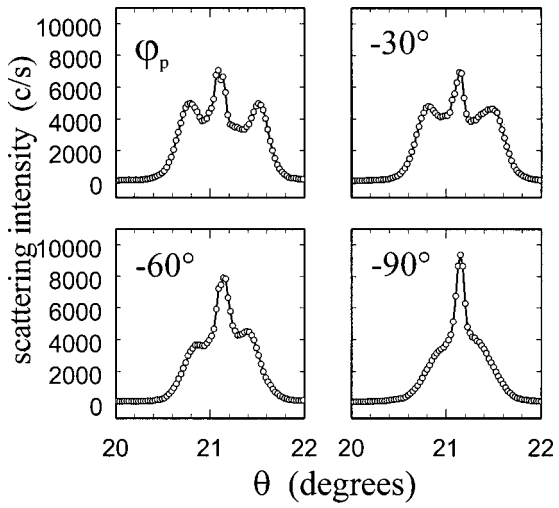

FIG. 8. Partially suppressed peak splitting for a sample grown at a moderate growth rate, with $T_{ss}=40.1\,^{\circ}\mathrm{C}$, $T_d=30\,^{\circ}\mathrm{C}$, and $\Delta=10.1\,^{\circ}\mathrm{C}$.

IV. ORIGIN OF THE TILTING

We are not able to image the microscopic structure of the RbI-mica interface directly, but a number of general predictions can be made on the basis of known properties of ionic solids and mica. As described in recent molecular dynamics simulations,[16] the muscovite mica cleavage surface contains oxygen tetrahedra in a distorted hexagonal array. In the bulk, potassium ions lie at the centers of all of the hexagons, but on cleavage it is likely that the potassium ions are equally distributed on each cleavage surface, preserving electrical neutrality and leaving half of the potassium sites unoccupied.[17]

In the rocksalt RbI structure, successive (111) planes are polar and occupied by either Rb or I. The mica K sites closely match the Rb sites and it is likely that the centers of the oxygen hexagons are occupied by Rb at the RbI-mica interface. Since we see no way in which iodine could be incorporated at the mica surface, we do not consider the possibility of an I-terminated RbI interface. Based on the foregoing considerations, we model the RbI interface as a set of Rb-terminated terraces separated by bilayer steps, as in the example of Fig. 11.

For an ionic crystal, the surface energy of polar terminating planes generally makes such surfaces unstable. In the case of the rocksalt structure, the low-energy faces are neutral {100} planes, and a polar (111) interface requires special consideration. The problem of electric fields and potentials at

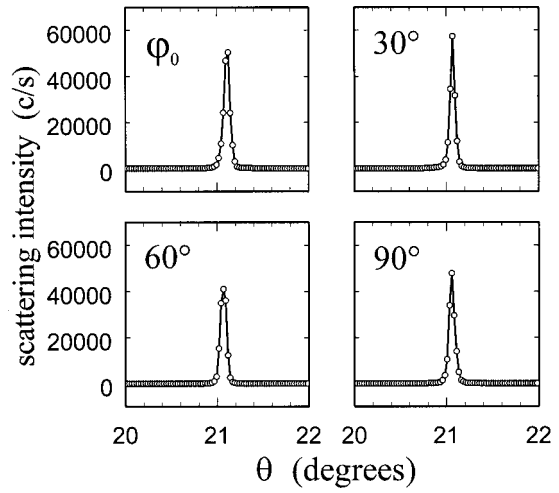

FIG. 9. θ scans for a sample grown at $T_{ss}=59.4\,^{\circ}\mathrm{C}$, $T_d=-8\,^{\circ}\mathrm{C}$, and $\Delta=67.4\,^{\circ}\mathrm{C}$, showing a complete suppression of interfacial tilting.

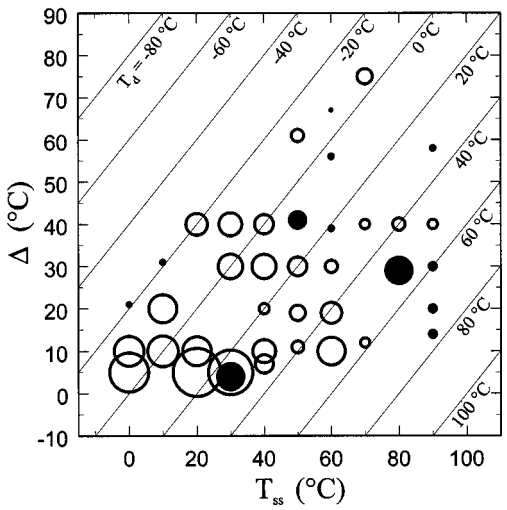

FIG. 10. Morphology map including samples prepared over the full range of growth conditions. Open circles correspond to samples that exhibit discrete tilt angles, with the diameter of the circles proportional to the peak splitting at ϕ_p. Filled circles correspond to samples with no peak splitting, with the diameter proportional to the peak width. The large filled circles correspond to samples with a continuous distribution of tilt angles and the small filled circles indicate samples in which the tilting is absent.

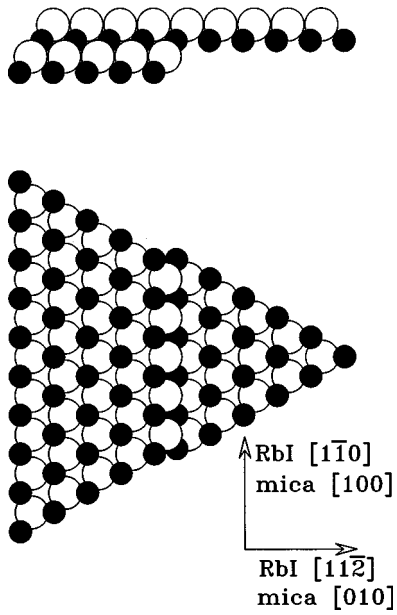

FIG. 11. Model of a RbI island with Rb (111) planes (filled circles) at the interface, shown in elevation (upper drawing) and from the substrate side (lower drawing). A bilayer step is shown with the step edge along RbI $[1\bar{1}0]$, corresponding to a tilt toward RbI $[11\bar{2}]$. The open circles correspond to iodine ions.

polar-compound–semiconductor interfaces was treated by Harrison *et al.*[18] and their method is directly applicable to the (111) face of RbI. (We initially discuss RbI in the absence of a mica substrate.) We treat the (111) planes as sheets with a uniform charge density $\sigma = 4e/(\sqrt{3}a^2)$, where a is the RbI lattice parameter. As in the example treated in Ref. 18, if the terminating Rb layer is fully occupied an average electric field will occur within the crystal and the potential will increase rapidly as a function of the distance from the interface. On the other hand, if the terminating Rb layer is half occupied its charge density drops to $\sigma/2$ and the average field in the crystal drops to zero. Although the average field is zero, there will be an average potential offset δ in the crystal, relative to the interface plane. For the RbI structure with a half-occupied terminating layer, $\delta = e/(6\kappa\epsilon_0 a)$, in SI units. Using a static dielectric constant $\kappa = 4.91$ for RbI,[19] we obtain a potential offset $\delta = 0.84$ V.

These arguments show that it is possible to modify the large electrostatic energies associated with polar surfaces by an appropriate modification of occupancies in the terminating layers. A lower-energy reconstruction of the (111) surface with a potential offset $\delta = 0$ can be obtained by setting the occupancies of the surface Rb and I layers to 0.25 and 0.75, respectively.[18] It is interesting to note that these occupancies correspond to those of the octopole reconstruction, which is thought to be the most stable modification of (111) rocksalt surfaces.[20]

Since our samples contain a RbI-mica *interface*, we next consider the juxtaposition of the RbI and mica crystals, with a fully occupied Rb layer at the interface. Half of the Rb ions can be assigned to the mica surface, replacing the K ions which stabilize the surface.[16,17] The other half of the Rb ions stabilizes the RbI surface, with a potential offset $\delta = 0.84$ V, as discussed above. While the octopole reconstruction seems favorable for a free RbI surface, we see no way in which it could be incorporated at the interface, except by including an array of vacancies, which seems unlikely.

Having shown that it is reasonable for the interface layer to consist of a fully occupied Rb layer, we next include the effects of misfit between the RbI and mica lattices, where the epitaxial orientation is such that RbI $[1\bar{1}0]$ is parallel to mica [100]. Along this direction, the miscut is given by

$$m_{100} = \frac{(1/\sqrt{2})a - a_m}{(1/\sqrt{2})a}.$$

Similarly, along mica [010] the miscut is

$$m_{010} = \frac{\sqrt{\frac{3}{2}}a - b_m}{\sqrt{\frac{3}{2}}a},$$

where a is the RbI lattice parameter and a_m and b_m are mica lattice parameters. Tilt effects are quite sensitive to the choice of lattice parameters, and as pointed out in Ref. 13 natural muscovite mica occurs with a range of compositions and lattice parameters. Therefore we consider a range of epitaxial misfits by using the RbI lattice parameter of Ref. 14 and both sets of quoted mica parameters in Ref. 13. Along mica [100] we find a misfit m_{100} ranging from -0.24% to -0.01%, and along mica [010] the misfit m_{010} varies from -0.29% to -0.26%. Since the x-ray measurements indicate a predominant tilt direction along mica [010] and RbI $\langle 11\bar{2}\rangle$, in the following discussion we restrict ourselves to a model of tilt that lies purely along that direction.

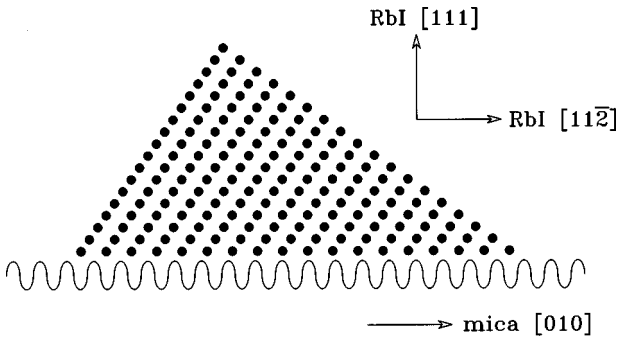

FIG. 12. Elevation drawing of Rb ions in the $(1\bar{1}0)$ plane of a RbI island. The substrate potential is indicated schematically, with an exaggerated misfit ($m_{010} = -1/15$). The Rb ions are in registry at the left and right edges of the island and out of registry at the center.

Figure 11 shows a bilayer step on a Rb-terminated crystal, viewed from the substrate side. The step edge is along RbI $[1\bar{1}0]$ and if this crystal was placed on a flat surface the tilt would be toward RbI $[11\bar{2}]$. Misfit accommodation is made possible by such steps because the Rb sites in the right-hand terrace are displaced horizontally, relative to the sites in the left-hand terrace. The same type of crystal is shown in a cross-sectional elevation view in Fig. 12, with the substrate potential indicated schematically by the oscillatory function below the crystal. For clarity, Fig. 12 shows only the Rb ions in a $(1\bar{1}0)$ plane of a RbI island which is terminated above by {100} faces. This island corresponds to one of the two possible stacking twins, with a right-left asymmetry that is evident. The second type of epitaxial island orientation would be generated by 180° rotation about the vertical axis, corresponding to the other possible fcc stacking twin. Figure 12 is drawn with an exaggerated misfit ($m_{010} = -1/15$) in order to show the gradual shift of Rb ions in and out of favorable sites. With this interface structure there is no net attractive interaction between the substrate and the overlayer.

A crystal with bilayer steps along RbI $[1\bar{1}0]$ (as in Fig. 11) is shown in an elevation view in Fig. 13, with the same

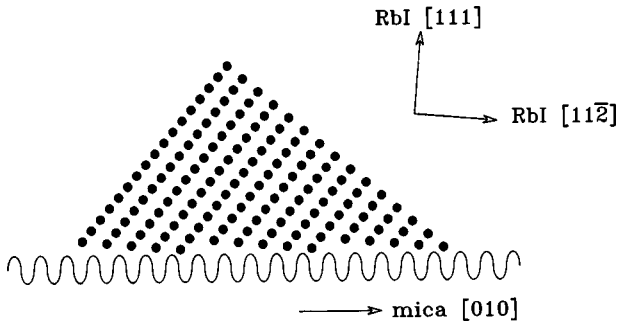

FIG. 13. Tilted RbI island on mica. Using the same lattice parameters as in Fig. 12, all interfacial Rb ions are brought into approximate registry by tilting the island toward Rb $[11\bar{2}]$ (mica [010]), with a tilt-angle criterion derived in the text.

misfit as in Fig. 12. In this case, where the misfit is negative, a tilt to the right helps to accommodate the misfit by putting nearly all of the interfacial Rb ions at favorable sites. On the other hand, positive misfit would be accommodated by a tilt to the left. The tilt direction also reverses if one considers islands with the second epitaxial orientation. These considerations show that the asymmetry of the fcc lattice favors the tilt of individual (untwinned) RbI islands along a specific direction. In a sample with both island orientations present, tilts will occur in both directions, leading to symmetric θ-scan profiles such as those of Fig. 3. The tilt angle depends on the magnitude of the misfit, and both tilt directions will occur regardless of the sign of the misfit; therefore it is not possible to determine the sign of the misfit from the x-ray measurements.

In order to calculate the optimum tilt angle for a given value of the misfit, we refer to Fig. 13 and assume that the misfit is negative. The distance between the substrate minima is b_m and the horizontal distance between Rb ions in a given (111) plane is $\sqrt{\frac{3}{2}}a$. If a given Rb ion lies at a potential minimum, its neighbor will be displaced from the adjacent minimum by a distance $b_m-\sqrt{\frac{3}{2}}a$. The displacement increases from site to site, until it becomes favorable to switch to the next Rb layer, where the ions are displaced to the right by the distance $a/\sqrt{6}$. (The switch corresponds to the inclusion of a bilayer step at the interface.) After n lattice steps, the translation associated with the bilayer step restores the perfect registry of the interfacial Rb ions. In this case, $n(b_m-\sqrt{\frac{3}{2}}a)=a/\sqrt{6}$ and $n=1/(3|m_{010}|)$. Solving for the misfit as a function of the tilt angle, we find $|m_{010}|=\tan\theta/\sqrt{2}$. For Fig. 13, where $m_{010}=-1/15$, this equation yields $\theta=5.4°$.

The data of Fig. 3 indicate a tilt angle along mica [010] of 0.42°; substitution of this value into our tilt model leads to a terrace width (in lattice units) of $n=64$ and a misfit $|m_{010}|\sim 0.5\%$. This value is approximately twice as large as the value calculated above using the published values of the lattice parameters; the discrepancy corresponds to an error of $\sim 0.25\%$ in lattice parameters, perhaps due to impurities in the RbI overlayer or in the mica.

Our interpretation of the data of Fig. 3 is that the samples contain an ensemble of RbI islands, with entire islands or macroscopic portions of the islands tilted along particular azimuths. The observed tilt directions are discrete, with the primary direction (at ϕ_p) toward mica [010], and the other tilt domains shifted by 30° and 60° in ϕ. The interface model that we have proposed accounts for misfit accommodation along mica [010] by interfacial ''switching'' to a lattice plane where the Rb ions are displaced along this direction. Since the bilayer-to-bilayer shift in site positions is purely along mica [010], this model does not provide misfit accommodation along mica [100]. On the other hand, the direction of the macroscopic *tilt* of the RbI islands is controlled by the direction of the step *edges*. In Fig. 11 we have shown a step edge along RbI $[1\bar{1}0]$, but step edges could also be oriented along symmetry-equivalent $\langle 1\bar{1}0\rangle$ directions (60° away in azimuth) or along RbI $\langle 11\bar{2}\rangle$ directions (30° away). Our model does not explicitly address the dynamics of overlayer tilting, but we speculate that bilayer steps are incorporated at the interface as the RbI overlayer spreads horizontally across the substrate.

Having discussed tilting mechanisms, we turn to the dependence on growth conditions which is summarized in Fig. 10. Each point in this figure corresponds to a single sample. Since run-to-run variations occur for samples grown under identical conditions, the tilt behavior as a function of growth conditions is not monotonic in this figure. Nonetheless, the general trend is that crystallographic tilting is suppressed when the substrate temperature is increased or when the growth rate is increased.

Given different thermal expansion coefficients for RbI and mica, the interfacial misfit is a function of temperature. The linear coefficient of thermal expansion of muscovite mica in the cleavage plane is approximately $10\times10^{-6}/°\mathrm{C}$.[21] Using the data of Ref. 22, we find an expansion coefficient for RbI of $39\times10^{-6}/°\mathrm{C}$, giving a differential thermal expansion of $29\times10^{-6}/°\mathrm{C}$. Since the calculated misfit is negative at room temperature, the misfit is reduced as the growth temperature is increased. In raising T_{ss} from 20 to 90 °C, the misfit would decrease by 0.2%, which may explain (at least in part) our observation of vanishing tilting at high growth temperatures.

The growth-rate dependence in Fig. 10 is most obvious for the sets of samples prepared at 0, 10, and 60 °C, where the tilting was significant at low growth rates and vanished at high rates. It is not clear from our measurements whether the samples grown at high rates have nonstepped pseudomorphic interfaces, or whether the misfit accommodation occurred through a symmetric (tilt-free) dislocation mechanism. Qualitatively, we speculate that the tilted interfaces represent an equilibrium structure, and that growth at high rates proceeds faster than tilted interfaces are able to form.

V. SUMMARY AND COMMENTS

The tilts along multiple azimuths discussed in this paper are somewhat complex, in comparison to those discussed by previous authors, but it is very likely that the basic driving force for tilt formation is misfit accommodation, as in the other cases. Our interface model exploits the asymmetry of the rocksalt structure and uses the formation of bilayer steps to relieve the misfit along mica [010]. Using previously published values of the lattice parameters of RbI and mica, the tilt angle predicted by our model does not match the measured tilt angles exactly, but it is probable that it is qualitatively correct.

Although tilting phenomena are well known in the literature, the study of ionic solids is relatively uncommon in surface science experiments. Nonetheless, epitaxial deposits of NaCl with (111) interface planes have been grown on Ge,[23] and GaAs.[24] In both cases the rocksalt structures grew as triangular pyramids with two orientations, similar to those of our experiments. Since no tilt measurements were reported by the authors of Refs. 23 and 24, it is unknown whether crystallographic tilts occurred in those cases.

The other unusual feature of the RbI system, namely, the inherent asymmetry of the overlayer crystal structure, is generally absent in previous studies of tilt phenomena, with only one exception that we are aware of. This is the case of hcp rare earths grown with $(10\bar{1}2)$ interface planes.[25] As with

RbI (111), the sign of the misfit favors the tilt of a given stacking twin along a particular direction. If the substrate was flat, both twins and therefore both tilt directions would be present, as in our case. Since the substrates used in Ref. 25 were intentionally miscut, the growth of one of the stacking twins was suppressed. To our knowledge, ours is the first report of tilting on a substrate with zero miscut.

ACKNOWLEDGMENTS

This project was supported by Research Corporation Grant No. CC4930, Petroleum Research Fund Grant No. 34562-B5, and the Wehr Foundation. Instrumental techniques were discussed with P. Micelli, and important technical support was provided by N. Schook and J. Meehl.

*Current address: Department of Physics, Boise State University, Boise, ID 83725-1570.

[1] S. A. de Vries, P. Goedtkindt, S. L. Bennett, W. J. Huisman, M. J. Zwanenburg, D.-M. Smilgies, J. J. De Yoreo, W. J. P. van Enckevort, P. Bennema, and E. Vlieg, Phys. Rev. Lett. **80**, 2229 (1998).

[2] H. Henry Teng, Patricia M. Dove, Christine A. Orme, and James J. De Yoreo, Science **282**, 724 (1998).

[3] Joanna Aizenberg, Andrew J. Black, and George M. Whitesides, Nature (London) **398**, 495 (1999).

[4] Jay A. Switzer, Mark G. Shumsky, and Eric W. Bohannan, Science **284**, 293 (1999).

[5] Th. Pauporté and D. Lincot, Appl. Phys. Lett. **75**, 3817 (1999).

[6] F. J. Lamelas, J. D. Schmidt, and May Xiong, Phys. Rev. B **58**, 14 270 (1998).

[7] Haruo Nagai, J. Appl. Phys. **45**, 3789 (1974).

[8] J. Kleiman, R. M. Park, and H. A. Mar, J. Appl. Phys. **64**, 1201 (1988).

[9] Ferenc Riesz, J. Varrio, A. Pesek, and K. Lischka, Appl. Surf. Sci. **75**, 248 (1994).

[10] F. K. LeGoues, P. M. Mooney, and J. Tersoff, Phys. Rev. Lett. **71**, 396 (1993).

[11] J. E. Ayers, S. K. Ghandhi, and L. J. Schowalter, J. Cryst. Growth **113**, 430 (1991).

[12] J. C. A. Huang and C. P. Flynn, Philos. Mag. Lett. **64**, 71 (1991).

[13] David R. Collins and C. Richard A. Catlow, Am. Mineral. **77**, 1172 (1992).

[14] Howard E. Swanson, Ruth K. Fuyat, and George M. Ugrinic, ''Standard X-Ray Diffraction Powder Patterns,'' Natl. Bur. Stand. (U.S.) Circ. No. 539 (U.S. GPO, Washington, DC, 1955), Vol. 4, p. 43.

[15] We know that the *individual* RbI islands are untwinned, since their macroscopic shapes are almost universally triangular.

[16] M. Odelius, M. Bernasconi, and M. Parrinello, Phys. Rev. Lett. **78**, 2855 (1997).

[17] R. F. Giese, Nature (London) **248**, 580 (1974).

[18] W. A. Harrison, E. A. Kraut, J. R. Waldrop, and R. W. Grant, Phys. Rev. B **18**, 4402 (1978).

[19] R. P. Lowndes, Phys. Lett. **21**, 26 (1966).

[20] Dieter Wolf, Phys. Rev. Lett. **68**, 3315 (1992).

[21] Lester Goldstein and Ben Post, J. Appl. Phys. **40**, 3056 (1969).

[22] K. K. Srivastava and H. D. Merchant, J. Phys. Chem. Solids **34**, 2069 (1973).

[23] S. Fölsch, U. Barjenbruch, and M. Henzler, Thin Solid Films **172**, 123 (1989).

[24] Koichiro Saiki, Yuji Nakamura, Naoshi Nishida, Wei Gao, and Atsushi Koma, Surf. Sci. **301**, 29 (1994).

[25] R. Du and C. P. Flynn, J. Phys.: Condens. Matter **2**, 1335 (1990).